44th AIAA Aerospace Sciences Meeting and Exhibit
9 - 12 January 2006, Reno, Nevada

AIAA 2006-1363

On the Study of Uncertainty in Inflow Turbulence Model Parameters in Wind Turbine Applications

Korn Saranyasoontorn* and Lance Manuel†

Dept. of Civil, Architectural and Environmental Engineering, University of Texas, Austin, TX 78712

In stochastic simulation of inflow turbulence random fields for wind turbine applications, one routinely employs standard spectral models specified in terms of parameters that are usually provided as fixed values. Recent studies suggest that these parameters can exhibit significant variability. As such, it is not unreasonable to expect that derived flow fields based on simulation with such spectral models can be in turn highly variable. Turbine load and performance variability could as well result. The aim here is to assess the extent of variability in derived inflow turbulence fields that arises from accounting for the noted variability in spectral model parameters. Simulation of these parameters as random variables forms the basis of this study. A commercial-sized 1.5MW concept wind turbine is considered in the numerical studies. The variability in turbulence power spectral density functions at points on the rotor plane and in turbulence coherence functions for separations on the order of a rotor diameter is studied. Using time domain simulations, statistics of various wind turbine response measures are also studied where the focus is on the variability in gross statistics such as root-mean-square response and ten-minute extremes. While variability in inflow turbulence spectra can be great, the variability in turbine loads is generally considerably lower. One exception is for turbine yaw loads whose larger variability arises from its sensitivity to a coherence decay parameter that is itself highly variable. Finally, because reduced-order representations of turbulence random fields using empirical orthogonal decomposition techniques can allow useful physical insights into spatial patterns of flow, variability in the energy distribution and the shapes of such empirical eigenmodes is studied and a simplified model is presented that retains key variable sources in a limited number of modes and that accurately preserves inflow turbulence field variability.

I. Introduction

When stochastic approaches are used in the design of a wind turbine, one routinely generates a wind velocity field over spatial dimensions on the scale of the turbine rotor diameter and in accordance with a prescribed spectral turbulence model. Employing such a simulated wind velocity field, one can then perform wind turbine response calculations, collect turbine load statistics, and finally extrapolate them to yield long-term design loads. It is clear then that the choice of spectral turbulence model and associated parameters used in generation of the inflow turbulence field can greatly influence predicted wind turbine design loads.

In the International Electrotechnical Commission (IEC) standard[1] for wind turbine design, the normal turbulence model assumes fixed spectral inflow parameters as a basis for stochastic simulation of the inflow turbulence field. Neutrally stable conditions are also usually assumed in such simulations. The expectation is that critical wind turbine loads occur at high wind speeds for which neutral atmospheric conditions may be assumed. However, significant turbulent energy may also occur over many hours each day under stable and unstable conditions as well; these conditions could then lead to large turbine loads. Especially over the planned service life of a wind turbine, consideration of these various atmospheric conditions can be important. Indeed, recent studies by Kelley et al[2,3] have demonstrated that significant fatigue damage can occur from coherent turbulence structures that develop in the stable, nocturnal atmospheric boundary layer.

*Graduate Research Assistant
†Associate Professor

Kelley et al[3] also point out that the non-stationarity of the wind velocity process, not represented in the IEC turbulence models, can be another important factor in predicting wind turbine loads. Notwithstanding the stated obvious limitations of doing so, we restrict our study of wind turbine loads to neutral atmospheric conditions and to use of normal turbulence models (similar to that prescribed in the IEC guidelines) and implied stationary flow fields. Our justification is that we wish to focus primarily on variability in the derived turbulence fields and in turbine loads in these conditions.

The IEC guidelines recommend the use of inflow turbulence models with prescribed (deterministic) spectral parameters. As a result, these models do not account for the inherent variability likely to be present in the spectral parameters. Evidence of this variability is seen in the large uncertainty in parameters estimated for turbulence field spectral and coherence models based on experimental measurements. Exponential coherence decay parameters reported in the literature, for instance, vary quite substantially, indicating uncertainty in describing the coherence structure of turbulence random fields at different frequencies and spatial separations. The variability in such inflow turbulence parameters is the subject of a review paper by Solari and Piccardo[4] that summarizes the findings from numerous experimental studies carried out over more than two decades. We believe that it is of interest to study the extent to which the variability of the spectral parameters propagates to variability in turbulence spectra as well as in turbine response statistics. It is also useful to develop a simplified and efficient approach for describing the variability in the inflow turbulence random field. We attempt to do this by employing empirically developed low-dimensional representations of this full turbulence field.

Based on the foregoing discussions, we devote the first part of this study to a review of the uncertainty in the spectral parameters that appear in the turbulence model of Solari and Piccardo.[4] Conveniently, estimates of statistical moments for all the parameters have been obtained from a large set of experimental measurements and are available for the present study. These parameter uncertainties lead to significant variability in cross-power spectral density (CPSD) functions as well as in covariance matrices for the atmospheric turbulence field. Using simulated turbulence spectra on a vertical plane with dimensions representing a commercial-sized 1.5MW wind turbine, we will show first that a considerable amount of variability in inflow turbulence spectra and coherence can indeed exist. Next, we evaluate the impact of the inflow spectral model parameter uncertainty on wind turbine structural responses. Time-domain simulations of the wind turbine response of a model of the virtual variable-speed 1.5MW turbine developed as part of the WindPACT study[5] are performed where the rotor is assumed to experience full-field wind velocity processes simulated based on the unified turbulence model of Solari and Piccardo.[4] The turbine response time histories are post-processed and the variability in the statistics (root-mean square levels and ten-minute extremes) of various turbine loads, including out-of-plane bending moment at the blade root, fore-aft tower bending moment at the base, and yaw moment at the tower top, are compared with the variability in inflow model parameters used in the simulations.

In the latter part of this study, we develop a simplified approach that attempts to account for important flow variations by means of an efficient approach that involves the use of low-dimensional representations of the turbulence random field. It has been demonstrated elsewhere by the authors[6] that turbine loads can often be accurately predicted by including only a small number of energetic "modes" empirically derived using Proper Orthogonal Decomposition (POD). Accordingly, we seek here to assess the variability in the energy and spatial distribution among the most important POD modes that results from variability in spectral model parameters. The use of POD in wind turbine applications is of particular interest because it can help in making physical interpretations of inflow patterns and relating these to turbine loads. Additionally and importantly, POD has the desired property of optimality over alternative decomposition schemes for spatio-temporal random fields and can thus yield highly efficient low-dimensional field representations for 3-D inflow turbulence for wind turbines. In recent studies, Spitler et al,[7] Lindberg et al,[8] and Saranyasoontorn and Manuel[6] have applied POD techniques to identify, characterize, and model energetic coherent patterns in turbulence fields. Results have confirmed the efficiency of the procedure for use over spatial scales of interest in wind turbine applications. However, the variability in the orthogonal eigenmodes (shapes) and in their associated kinetic energy contributions (or eigenvalues) have not been studied in any systematic manner. A preliminary investigation of this variability is the focus of this study; POD procedures permit easy separation of the variability from these two sources and thus make the modeling of uncertainties convenient.

II. Variability in Inflow Parameters, Turbulence Spectra, and Turbine Loads

A. Unified turbulence model of Solari and Piccardo[4]

In a recent study, Solari and Piccardo[4] published a critical review on the selection of and variability in parameters that appear in spectral models used to represent three-dimensional atmospheric turbulence structure. Data from numerous reliable experimental measurements of turbulence in flat homogeneous terrain and near-neutral atmospheric conditions were utilized to estimate the first two marginal statistical moments of each spectral model parameter and in some cases correlation coefficients among pairs of parameters. In terms of ϵ used to represent a single turbulence component in the along-wind (u), across-wind (v), or vertical (w) direction, and r used to indicate the Cartesian coordinate (x, y, or z) in which a separation distance is expressed, the various spectral model parameters studied by Solari and Piccardo[4] included (i) turbulence intensity factors, β_ϵ, (ii) parameters related to the integral length scales of the turbulence, ξ_ϵ, (iii) exponential decay coefficients, $C_{r\epsilon}$, of coherence functions based on the Davenport model,[9] and (iv) a point cross-coherence scaling factor between u and w, κ_{uw}. The available data revealed large variability in some of these estimated parameters; for instance, estimates of the coefficient of variation (COV) of the exponential decay parameter $C_{r\epsilon}$ was found to be as high as 60%. Based upon the reliable data sets, Solari and Piccardo expressed the first two marginal statistical moments of most of these parameters as functions of only one (assumed) deterministic input: the roughness length, z_0. The correlation coefficient between distinct turbulence intensity factors, β_ϵ (namely $\rho(\beta_\epsilon, \beta_{\epsilon'})$) was found to be around 0.75. In the same manner, $\rho(\xi_\epsilon, \xi_{\epsilon'})$ and $\rho(C_{r\epsilon}, C_{r'\epsilon'})$ are 0.65 and 0.50, respectively.

Using two deterministic inputs—the roughness length, z_0, and the friction velocity, $u_\star$—together with the random variables, β_ϵ and ξ_ϵ, the power spectral density function of turbulent flow in the three directions can be expressed as a function of height and frequency. The random variables, $C_{r\epsilon}$ and κ_{uw}, are utilized to compute coherence and cross-power spectral density functions. This, then, forms a complete second-order statistical description of the multi-dimensional atmospheric turbulence random field that will be used extensively in the following. For the sake of brevity, detailed summaries of all the statistics and mathematical expressions for the turbulence model parameters are not included here but are summarized in the Appendix.

We demonstrate next, by using a wind turbine example, how uncertainty in the flow parameters (i.e., in β_ϵ, $C_{r\epsilon}$, κ_{uw}, and ξ_ϵ) affects uncertainty in estimates of turbulence power and coherence spectra. Later, we discuss the propagation of this uncertainty to the variability in wind turbine load statistics.

B. Variability of the inflow spectral model parameters

We take advantage of available results from the statistical studies by Solari and Piccardo[4] to study the variability of the different inflow spectral model parameters. The roughness length, z_0, considered deterministic, is assumed to be 0.05 m. For illustration purposes, twenty different sets of the model parameters are randomly generated. These simulations are carried out using the Latin Hypercube Sampling (LHS) technique[10] rather than the more conventional Monte Carlo simulation (MCS) technique since a reasonably representative distribution can be obtained even when only a limited number of data sets are sampled (twenty, in this particular case). Given the first two statistical moments of each parameter and, in some cases, correlation coefficients among pairs of parameters, these model parameters are assumed to follow a multivariate lognormal probability distribution. The lognormal model guarantees positive values for all of the sampled parameters. Table 1 lists the set of 20 LHS samples of the thirteen inflow parameters along with estimates of the sample means and coefficients of variation (COV). Also shown are sample mean and COV estimates if the 20 samples were obtained using MCS. To highlight the efficiency of the LHS over the MCS technique for the limited number of simulations used here, target mean and COV values are included in Table 1. It can be seen that, by using the LHS scheme,the estimated mean and COV of each model parameter is fairly close to the target value even though only 20 simulations are performed. The turbulence intensity factor for the along-wind component, β_u, for example, has target mean and COV values of 6.98 and 0.25, respectively, while the LHS sample mean and COV estimates found in Table 1 are 6.92 and 0.23, respectively.

C. Variability of the inflow turbulence spectra

We now investigate the uncertainty of the inflow turbulence spectra that results from the use of the spectral model and associated parameter variability as presented by Solari and Piccardo[4] with details summarized in the Appendix. For the twenty sets of LHS-simulated spectral model parameters presented in Table 1,

Table 1. Twenty simulated sets of inflow spectral model parameters based on Latin Hypercube Sampling (LHS) along with estimates of their means and coefficients of variation (COV). The roughness length, z_0, is 0.05 m. COV values are expressed in percentage. Monte Carlo Simulation (MCS) statistics for twenty simulations are shown only for comparison. Target mean and COV values based on Solari and Piccardo[4] are also included.

Run	β_u	β_v	β_w	ξ_u	ξ_v	ξ_w	κ_{uw}	C_{yu}	C_{yv}	C_{yw}	C_{zu}	C_{zv}	C_{zw}
1	6.67	4.90	1.16	1.38	0.34	0.15	2.03	11.60	5.45	5.23	9.74	6.79	2.49
2	5.07	3.09	1.85	1.07	0.22	0.07	1.54	5.31	2.78	3.38	8.08	4.90	2.87
3	5.65	3.21	1.08	1.24	0.38	0.13	1.79	8.43	3.58	5.17	9.07	5.64	2.74
4	8.26	3.64	1.60	0.93	0.31	0.08	3.22	12.58	8.76	4.80	7.00	5.45	2.50
5	5.28	3.26	1.31	1.00	0.18	0.07	3.85	14.92	10.26	7.40	12.78	8.83	3.04
6	10.17	5.46	2.69	0.84	0.25	0.08	1.90	9.48	9.03	5.61	8.72	7.09	2.38
7	7.23	2.67	1.98	0.82	0.15	0.11	2.22	19.98	5.66	10.66	13.71	9.17	4.61
8	4.27	2.11	0.94	0.40	0.13	0.06	2.43	7.84	3.14	4.37	9.83	6.37	2.88
9	6.23	2.85	1.47	0.67	0.11	0.05	2.12	13.81	12.18	11.93	7.92	6.46	3.39
10	7.57	3.88	2.17	1.01	0.19	0.12	3.41	10.07	17.82	6.04	10.62	8.14	3.25
11	6.12	4.64	1.38	0.89	0.19	0.10	2.69	5.68	7.24	3.97	9.51	5.08	2.98
12	8.61	4.45	1.23	0.76	0.29	0.09	1.93	16.00	6.42	6.84	11.72	6.91	3.78
13	5.95	3.49	1.69	1.25	0.33	0.14	1.75	10.36	7.52	8.33	11.22	5.77	3.59
14	8.00	4.27	2.06	1.13	0.26	0.07	2.58	6.42	4.78	8.50	10.20	7.29	2.65
15	8.75	6.78	3.37	0.86	0.21	0.10	2.48	6.84	2.63	4.10	8.53	5.94	2.15
16	6.40	3.78	1.75	1.17	0.22	0.09	1.69	11.27	5.11	9.39	11.07	7.74	3.88
17	7.04	4.11	1.95	0.73	0.17	0.06	2.87	8.25	4.11	6.61	12.22	6.19	3.15
18	9.35	5.78	2.40	1.47	0.47	0.21	2.36	9.25	6.26	7.08	10.45	6.55	3.29
19	4.90	2.36	1.59	0.96	0.27	0.12	3.10	7.21	4.37	5.91	9.23	5.32	2.71
20	6.97	2.60	1.51	1.07	0.24	0.09	2.16	3.70	1.76	3.10	7.34	4.57	2.07
LHS-Mean	6.92	3.87	1.76	0.98	0.25	0.10	2.41	9.95	6.44	6.42	9.95	6.51	3.02
LHS-COV	22.8	31.4	33.4	25.9	35.8	38.7	26.0	40.4	59.1	37.4	18.2	19.5	20.7
MCS-Mean	6.31	3.40	1.64	0.97	0.26	0.10	2.34	9.34	5.83	5.75	9.46	6.21	2.72
MCS-COV	21.4	20.2	22.8	23.6	43.0	37.6	24.7	36.2	43.5	38.4	19.1	16.7	17.8
Target Mean[4]	6.98	3.84	1.75	1.00	0.25	0.10	2.44	10.00	6.50	6.50	10.00	6.50	3.00
Target COV[4]	25.0	32.8	32.2	25.0	39.0	38.7	30.0	40.0	60.0	40.0	20.0	20.0	20.0

power spectral density (PSD) functions and coherence functions of the inflow turbulence are computed. A roughness length, z_0, of 0.05 m and a friction velocity, u_*, of 1.0 m/s are assumed. In order to have an illustrative example and scale that are representative of a commercial wind turbine, we compute PSD and coherence functions at an elevation of 84 m above the ground. This elevation is consistent with the hub height of the wind turbine that will be studied later. Figure 1 shows the variations in 20 sample normalized PSD functions, $fS_{\epsilon\epsilon}$, for the along-wind (u), across-wind (v), and vertical (w) turbulence components. In the same fashion, Fig. 2(a-c) shows the variations in "space" coherence functions, $\Omega_{\epsilon\epsilon}$, for each of the three turbulence components at a lateral separation of 80 meters, which is close to the diameter of the wind turbine mentioned. Finally, the "point" coherence function between the u and w turbulence components, Γ_{uw}, at the same elevation is shown in Fig. 2(d). It is apparent from these figures that the sample PSD and coherence functions exhibit significant variability that arises from the variability in the spectral model parameters. For example, peaks in the normalized PSD of the along-wind (u) turbulence component vary from about 0.9 to 2.2 $(\text{m/s})^2$. Uncertainty in coherence function estimates at the 80-meter lateral separation is also significant especially for the across-wind (v) component. The relative variability in these coherence spectra for the different turbulence components is consistent with the variability or COV values of C_{yu}, C_{yv}, C_{yw} as can be confirmed from Table 1.

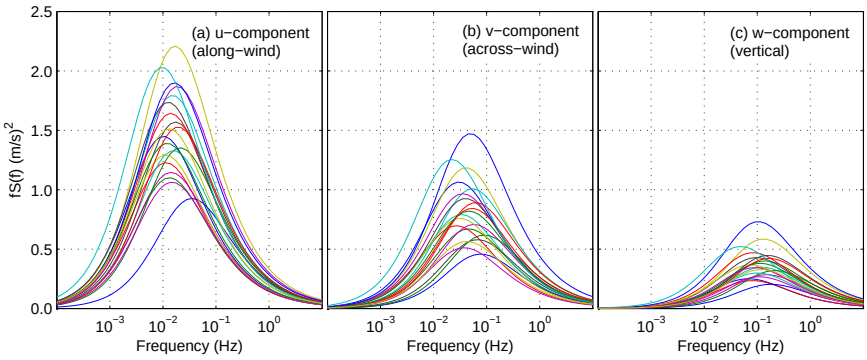

Figure 1. Sample normalized power spectral density functions of the three turbulence components (u, v, and w) at an elevation of 84 m above the ground derived using the twenty sets of simulated spectral model parameters in Table 1.

D. Variability of the wind turbine load statistics

We turn next to a case study of the impacts of variability in inflow spectral model parameters on wind turbine structural response or loads. The wind turbine loads we focus on are the out-of-plane bending moment at the root of a blade (BBM), the fore-aft tower bending moment at the base (TBM), and the yaw moment at the tower top (YM) for a model of a turbine that was developed as part of the WindPACT (Wind Partnerships for Advanced Component Technology) study.[5] This "virtual" turbine is a 1.5MW, variable-speed, 3-bladed, upwind, horizontal-axis turbine with a hub height of about 84 m and a rotor diameter of approximately 70 m. A sketch of this turbine is shown in Fig. 3.

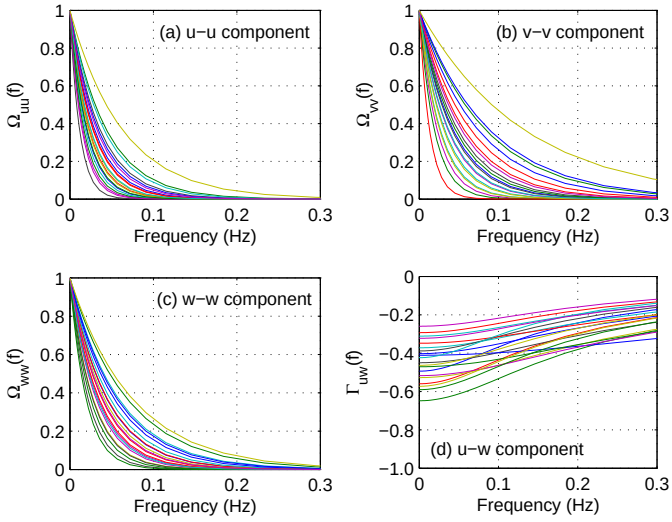

Figure 2. Sample coherence functions at an elevation of 84 m above the ground derived using the twenty sets of simulated spectral model parameters in Table 1. (a-c) "space" coherence functions for a lateral separation of 80 m., (d) "point" coherence functions between u and w components.

Based upon the Veers approach,[11] a MATLAB computer code was written for the generation of full-field, multivariate wind velocity processes on a 7×7 square grid that covers the entire rotor plane of the WindPACT turbine as shown in Fig. 3. To reflect the variability in inflow turbulence spectral parameters, twenty cross-power spectral density (CPSD) matrices associated with the twenty sets of simulated inflow parameters discussed earlier are computed. For each CPSD matrix, fifteen separate 10-minute wind velocity time series are first simulated, and then utilized for turbine response calculations made possible using the turbine simulator software FAST[12] (Fatigue, Aerodynamics, Structures, and Turbulence). This procedure therefore leads to a total of $20 \times 15 = 300$ 10-minute inflow/turbine response simulations.

Figure 4 shows typical time histories of the wind velocities at hub center in the along-wind ($\bar{u} + u$), across-wind (v), and vertical (w) directions. Also shown are time histories for various wind turbine response measures including the out-of-plane blade root bending moment (BBM), fore-aft tower bending moment at the base (TBM), yaw moment at the tower top (YM), blade tip displacement (BTD), and tower top displacement (TTD). Only a 100-second time segment is shown so as to focus on differences in the nature of the different time-varying quantities. As one might anticipate, the out-of-plane blade bending loads are strongly correlated with blade tip deflections while the fore-aft tower bending moment is strongly correlated with tower top deflections. Further study of the various turbine load time series suggests that the relatively

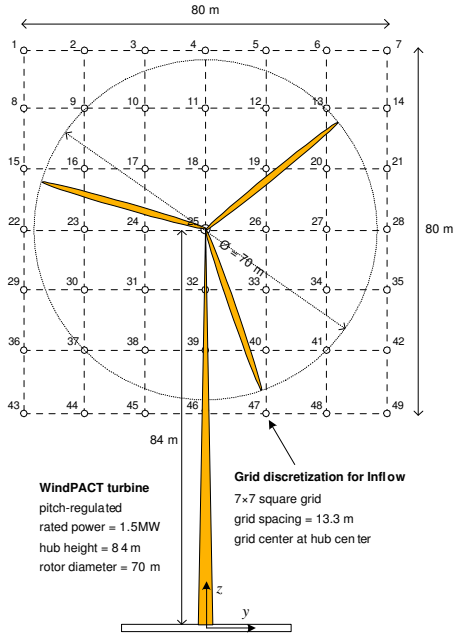

Figure 3. A schematic diagram of the WindPACT[5] turbine overlayed by a 7×7 square grid used in the inflow turbulence simulations.

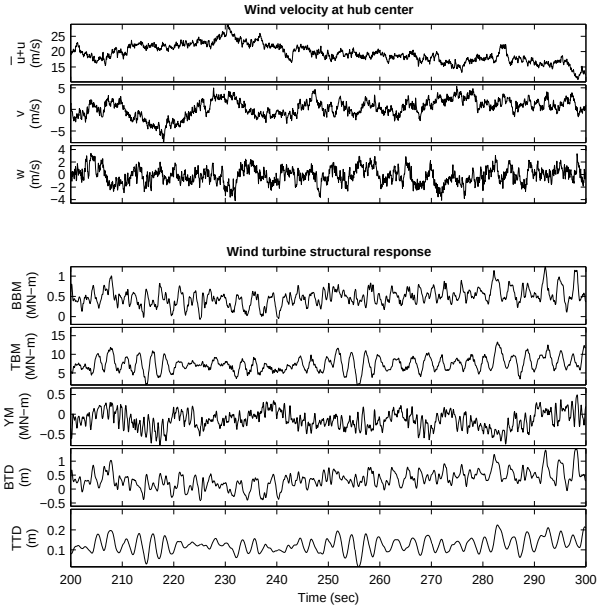

Figure 4. Typical time histories of the wind velocities, $\bar{u}+u$, v, and w, at the hub center (first three plots) and the turbine response measures, BBM, TBM, YM, BTD, and TTD (next five plots). (Note that BBM is the out-of-plane blade root bending moment, TBM is the fore-aft tower bending moment at the base, YM is the yaw moment at the tower top, BTD is the blade tip displacement, and TTD is the tower top displacement.)

larger high frequency content in YM relative to that in BBM and TBM as can be verified in Fig. 4 arises from rotational sampling at the $3P$ frequency (where P is the rotational frequency of the rotor) which is not a dominant frequency for BBM and TBM.

To investigate the variability in statistics of turbine loads (BBM, TBM, and YM), simulation-based

mean estimates of the root-mean-square value (RMS), and of the 10-minute extreme turbine loads (ext_{10}), are obtained from fifteen 10-minute turbine response time histories, for each of the 20 LHS-simulated input parameter sets. These estimates are summarized in Table 2 along with corresponding values of a few selected inflow parameters (β_u, ξ_u, κ_{uw}, and C_{yu}). The selected inflow parameters represent a single one (the most important) from among the four sets of random parameters discussed in the Appendix. Mean and COV estimates of these parameters as well as those of turbine load statistics are given in the table for comparison. From the table, it is clear that the variability in turbine load statistics is considerably smaller than that of the inflow parameters. For instance, the COV of the estimate of the RMS of BBM is only 1.2% while the COV of each of the inflow parameters in Table 2 is greater than 20%. In fact, for the two loads, BBM and TBM, COV estimates for RMS and extremes are never greater than 7%. In contrast, yaw load (YM) statistics are more variable with COV values for RMS and ext_{10} equal to 12.7% and 13.4%, respectively. These results suggest that turbine load statistics variability depend on the load type being considered. Yaw loads are introduced by the imbalance of aerodynamic forces on the turbine rotor[13] and thus are more sensitive to inflow coherence decay parameters, $C_{r\epsilon}$. Larger variability in $C_{r\epsilon}$ (for example, the 40% COV in the decay parameter related to C_{yu}, which is associated with coherence in along-wind turbulence, u, for different lateral separations, y) than in other inflow parameters (such as the three shown in Table 2) might explain why yaw moment statistics exhibit greater variability than the out-of-plane bending moment at the blade root (BBM) and the fore-after tower bending moment at the base (TBM).

In summary, the variability in wind turbine load statistics is rather insignificant compared to the considerably larger variability in some inflow parameters as suggested by Solari and Piccardo[4] and based on turbulence field measurements. Nevertheless, some load types, such as turbine yaw loads that depend on inflow parameters with especially large uncertainty, are relatively more variable than others. As a consequence, in the derivation of design loads for wind turbine components, at least for some load types, it might be important in probabilistic approaches to carefully account for inflow parameter variability in simulation of inflow turbulence and turbine loads.

III. Modeling Uncertainties in the Inflow Turbulence Field using POD

We have thus far demonstrated that there can be significant variations in the flow characteristics over the rotor plane of the 70-meter WindPACT machine by using second-moment statistics of the inflow turbulence field, i.e., the power spectral density and coherence functions. Such variability may need to be accounted for if one employs a stochastic approach for design of a wind turbine. In the following, we illustrate such variations of the flow in a more physically interpretable fashion. Here the variability in flow characteristics is described through the variability that propagates to specific derived inflow "patterns" or "modes" and kinetic energies associated with such patterns. This will be achieved through the use of Proper Orthogonal Decomposition (POD) techniques. Only the key concepts of POD will be briefly discussed in this paper; the theoretical background related to POD techniques and their use can be readily found in the literature.[14–16]

A. Proper Orthogonal Decomposition

In one form of Proper Orthogonal Decomposition, called in some places Covariance Proper Transformation (CPT), assume that one is given N weakly stationary zero-mean correlated random processes $\boldsymbol{V}(t) = \{V_1(t), V_2(t), \ldots V_N(t)\}^T$ and a corresponding $N \times N$ covariance matrix, $\mathbf{C_V}$. It is possible to diagonalize $\mathbf{C_V}$ so as to obtain the (diagonal) matrix, $\boldsymbol{\Lambda}$.

$$\boldsymbol{\Phi}^T \cdot \mathbf{C_V} \cdot \boldsymbol{\Phi} = \boldsymbol{\Lambda}; \quad \mathbf{C_V} \cdot \boldsymbol{\Phi} = \boldsymbol{\Phi} \cdot \boldsymbol{\Lambda}; \quad \boldsymbol{\Lambda} = \text{diag}\{\lambda_1, \lambda_2, \ldots \lambda_N\}. \tag{1}$$

The eigenvectors, $\boldsymbol{\Phi} = [\boldsymbol{\phi}_1, \boldsymbol{\phi}_2, \ldots \boldsymbol{\phi}_N]$ of $\mathbf{C_V}$ describe orthogonal basis functions in a principal space. It is then possible to rewrite the original N correlated processes, $\mathbf{V}(t)$, in terms of N uncorrelated *scalar* processes, $\boldsymbol{Z}(t) = \{Z_1(t), Z_2(t), \ldots Z_N(t)\}^T$ such that

$$\boldsymbol{V}(t) = \boldsymbol{\Phi} \cdot \boldsymbol{Z}(t) = \sum_{j=1}^{N} \boldsymbol{\phi}_j Z_j(t) \tag{2}$$

where the uncorrelated scalar processes can be derived by employing the orthogonality property,

Table 2. Mean estimates of the root-mean-square (RMS) and 10-minute extreme (ext_{10}) of turbine loads (BBM, TBM, and YM) based on 15 wind turbine response simulations carried out for each of the twenty sets of LHS-simulated inflow parameters in Table 1. The mean and coefficient of variation (COV) values based on the twenty sets of simulations are also shown. Inflow parameters β_u, ξ_u, κ_{uw}, and C_{yu} are included for comparison.

	Inflow parameters				RMS			ext_{10}		
Run	β_u	ξ_u	κ_{uw}	C_{yu}	BBM	TBM	YM	BBM	TBM	YM
1	6.67	1.38	2.03	11.60	574	8086	238	1230	14219	894
2	5.07	1.07	1.54	5.31	566	8091	196	1149	14137	742
3	5.65	1.24	1.79	8.43	567	8062	212	1193	13680	747
4	8.26	0.93	3.22	12.58	578	8115	277	1336	15923	1015
5	5.28	1.00	3.85	14.92	566	8030	223	1162	13056	810
6	10.17	0.84	1.90	9.48	589	8175	297	1422	16139	1161
7	7.23	0.82	2.22	19.98	573	8033	274	1262	14297	1013
8	4.27	0.40	2.43	7.84	562	8044	210	1142	13762	773
9	6.23	0.67	2.12	13.81	571	8078	257	1239	14489	960
10	7.57	1.01	3.41	10.07	576	8087	251	1337	14605	909
11	6.12	0.89	2.69	5.68	571	8109	215	1212	14469	816
12	8.61	0.76	1.93	16.00	579	8077	294	1371	14652	1070
13	5.95	1.25	1.75	10.36	569	8051	221	1185	13400	835
14	8.00	1.13	2.58	6.42	578	8142	236	1303	15579	903
15	8.75	0.86	2.48	6.84	582	8176	263	1378	16051	1002
16	6.40	1.17	1.69	11.27	571	8059	230	1296	14091	867
17	7.04	0.73	2.87	8.25	573	8086	241	1307	15095	911
18	9.35	1.47	2.36	9.25	583	8139	258	1392	15907	965
19	4.90	0.96	3.10	7.21	565	8051	203	1185	13565	736
20	6.97	1.07	2.16	3.70	573	8181	206	1258	15543	758
Mean	6.92	0.98	2.41	9.95	573	8094	240	1268	14633	894
COV(%)	22.8	25.9	26.0	40.4	1.2	0.6	12.7	6.8	6.5	13.4

$$\boldsymbol{Z}(t) = \boldsymbol{\Phi}^T \cdot \boldsymbol{V}(t). \tag{3}$$

Note that both $\boldsymbol{V}(t)$ and $\boldsymbol{Z}(t)$ are $N \times 1$ column vectors comprised of time-varying scalar processes.

The covariance matrix for $\boldsymbol{Z}(t)$, namely $\mathbf{C_Z}$, is equal to the diagonal matrix, $\boldsymbol{\Lambda}$, and an energy measure associated with each $Z_j(t)$ can be given in terms of its variance, λ_j. The original random processes are conveniently decomposed into N uncorrelated random processes. If the eigenvalues, $\boldsymbol{\Lambda}$, are sorted in decreasing order, a reduced-order representation, $\hat{\boldsymbol{V}}(t)$, is obtained by retaining only the first M covariance-based POD modes as follows:

$$\hat{\boldsymbol{V}}(t) = \sum_{j=1}^{M} \boldsymbol{\phi}_j Z_j(t) \quad \text{where} \quad M < N. \tag{4}$$

Two attractive features of the POD procedure for used in wind turbine applications are that (i) it provides physical interpretations for the spatial modes (inflow turbulence patterns) and (ii) the derived low-dimensional representation of the turbulence field is optimal compared to any other linear orthogonal decomposition.[14–16]

B. Uncertainty in POD Mode Shapes and Associated Kinetic Energy

We investigate next the uncertainty in eigenmodes $\boldsymbol{\phi}_j$ and eigenvalues λ_j derived based on Covariance Proper Transformation (CPT). The procedure and results discussed below can be extended in a straightforward manner to applications involving frequency-dependent eigenmodes derived using a CPSD matrix (this type of POD is sometimes termed Spectral Proper Transformation).

For each inflow turbulence component, we first define the total kinetic energy of the field as $E = trace(\mathbf{C_V})$. Because of the invariance property of the covariance matrix trace upon linear transformation, E is equal to $\sum_{j=1}^{N} \lambda_j$, where N is the total number of POD modes. The kinetic energy is non-negative and hence $E \geq 0$. Also, because the covariance matrix is positive definite, $\lambda_j \geq 0$, for all j. If we define the proportion of the total kinetic energy carried by each POD mode (effectively, the dimensionless eigenvalue) as $\alpha_j = \lambda_j / E$, for $j = 1, 2, \ldots N$, these modal energy proportions, α_j, are subject to the constraints $\alpha_j \geq 0$, for all j and $\sum_{j=1}^{N} \alpha_j = 1$. Normalizing the eigenvalues in this manner helps to simplify the procedure for modeling them as random variables. The decomposition of the covariance matrix of the inflow turbulence field shown in Eq. (1) can now be rewritten as:

$$\mathbf{C_V} = \sum_{j=1}^{N} \lambda_j \boldsymbol{\phi}_j \boldsymbol{\phi}_j^T = E \sum_{j=1}^{N} \alpha_j \boldsymbol{\phi}_j \boldsymbol{\phi}_j^T. \tag{5}$$

As a consequence of the above definitions, it is clear that turbulence field variability as reflected in second-moment statistics (i.e., in the covariance matrix) can be also understood in terms of variability from three sources. These include (i) the individual mode shapes, $\boldsymbol{\phi}_j$, (ii) the proportion of the kinetic energy, α_j, in each mode, and (iii) the total kinetic energy in the entire turbulence field, E. To accurately describe the overall uncertainty in the inflow turbulence field, the variability from all three of these sources needs to be accounted for. However, because of the desirable optimality properties of POD schemes discussed earlier, some modes may be disregarded thus yielding a simplified model without introducing significant error. This will be illustrated next.

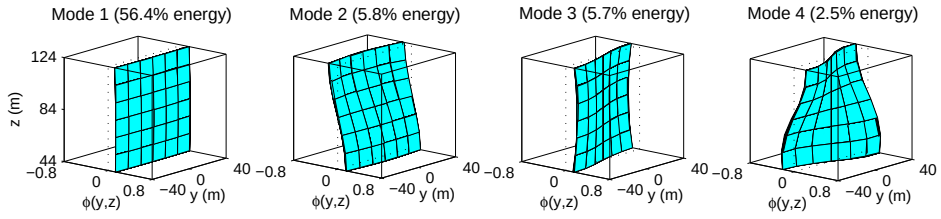

Figure 5. Twenty estimates of the first four POD mode shapes for the along-wind turbulence component based on twenty Latin Hypercube simulated samples of spectral model parameters.

To demonstrate the variability of the POD quantities discussed, i.e., $\boldsymbol{\phi}_j$, α_j, and E, the twenty sample CPSD matrices that were used earlier for inflow simulations over the rotor plane of the WindPACT turbine are again used to derive sample covariance matrices. Recall that these CPSD matrices are based on the turbulence model of Solari and Piccardo and were computed using the spectral parameter estimates shown in Table 1. For illustration purposes, the covariance matrices associated only with the along-wind (u) turbulence component are considered. Using the twenty sample 49×49 covariance matrices, POD eigenmodes and eigenvalues are computed. Thus, twenty sets of 49 eigenmodes, $\boldsymbol{\phi}_j$, 49 normalized eigenvalues, α_j, and the total kinetic energy, E, are obtained along with their corresponding mean values, $\bar{\boldsymbol{\phi}}_j, \bar{\alpha}_j$, and $\bar{E}$. For the first four POD modes, sample mode shapes from twenty simulations are shown in Fig. 5 along with the mean percentage of energy in each mode. It can be seen that the most energetic POD mode (Mode 1 in the figure) has an almost uniform shape. The next two modes exhibit roughly vertical and lateral sheared patterns, respectively, with about the same levels of kinetic energy, while the fourth mode is more complex. As can be verified upon studying the figure, the first four eigenmode shapes do not vary significantly with spectral model parameter variability. Higher mode shapes will generally exhibit greater variability but these higher modes will also contribute less towards the total energy. Hence, as an approximation, it may be acceptable to treat the random eigenmodes, $\boldsymbol{\phi}_j$, as fixed (non-varying) by using their mean shapes, $\bar{\boldsymbol{\phi}}_j$, to represent them.

The uncertainty in the non-dimensional kinetic energies, α_j, of the first twenty energetic modes from twenty realizations is studied in Fig. 6. The mean values of α_j based directly on the model proposed by Solari and Piccardo are shown as circles. Also shown are the maximum and minimum values of α_j from the simulations. It is clear that α_1 has considerable variability—in this case, it varies from approximately 43% to 68% of the total energy of the entire along-wind turbulence field. Note that the α_j values exhibit considerably smaller variability for all but the first mode (i.e., $j > 1$). We will use this fact later to propose an approximate model to represent uncertainties in the inflow field.

The total kinetic energy, E, is found to be quite variable, with an average energy (at each grid point) of about 6.9 $(\text{m/s})^2$ and a COV of 23%. By comparing with Table 1, it can be seen that these estimates are consistent with the statistics of β_u which is a parameter that is directly related to the variance of the along-wind turbulence field.

From the preceding discussions, it is clear that uncertainties in E and α_j need to be incorporated in any model that aims to accurately reflect the true variability in the overall turbulence field. This variability in E and α_j should probably be represented jointly; however, this is not discussed here. Additionally, because of the efficiency inherent in the POD procedure, higher POD modes are less energetic and therefore become less significant in terms of energy contributions. As such, large errors are not introduced if fixed (non-random) values based on the "mean" energy proportion, $\bar{\alpha}_j$, are assigned instead of the actual energy, α_j, for any higher (and less energetic) mode, j. We propose next a simplified model for the turbulence field variability that is developed based on the preceding discussions.

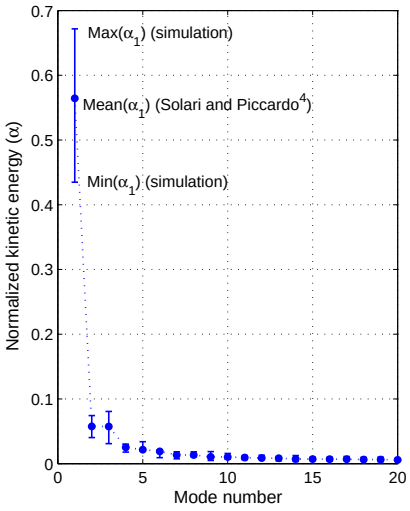

Figure 6. Mean values of the non-dimensional kinetic energy, α_j, for the first twenty POD modes (based on the model by Solari and Piccardo) of the along-wind turbulence field and maximum and minimum values from twenty simulations.

C. An Approximate Model for Uncertainties in the Inflow Turbulence Field

We have seen that the variability in the first few energetic POD mode shapes may be considered small (see Fig. 5). As a consequence, the "mean" mode shapes, $\bar{\boldsymbol{\phi}}_j$, that could be derived from field measurements, may be considered good representations for the true generally variable shapes if one wishes to construct a simplified model for the inflow turbulence field. Then, the variability in the flow characteristics would arise entirely from uncertainties in the kinetic energy (E and α_j). A further simplification can be made to the model by recognizing, based on Fig. 6, that (i) higher POD modes are in general less important to the turbulence field in terms of their kinetic energy contribution, and (ii) the variability of the energy proportion, α_j, in these higher modes is relatively small. Then, probability distributions for the total energy, E, and the normalized eigenvalues, α_j, of only the first few POD modes (say $j = 1, 2, \ldots, M$, where $M < N$) would be needed for the simplified model. In establishing such probability distributions, one should recall that these random variables are subject to the constraints: $E \geq 0$, $\alpha_j \geq 0$ for all j, and $\sum_{j=1}^{M} \alpha_j < 1$. For the higher POD modes, j (where $j > M$), as an approximation, the actual proportion of kinetic energy, α_j, may be replaced by the "mean" proportion of energy in such modes, $\bar{\alpha}_j$. Finally, then, these various approximations allow a rewriting of Eq. (5) as the following simpler mathematical expression:

$$\mathbf{C_V} = E\Big(\sum_{j=1}^{M} \alpha_j \bar{\boldsymbol{\phi}}_j \bar{\boldsymbol{\phi}}_j^T + \sum_{j=M+1}^{N} \bar{\alpha}_j \bar{\boldsymbol{\phi}}_j \bar{\boldsymbol{\phi}}_j^T\Big). \tag{6}$$

Small discrepancies may be expected between the mean level of the reconstructed covariance matrix based on the reduced-order POD representation with the other approximations implied by Eq. (6) and the target covariance matrix derived directly from simulated data (i.e., simulated values of the spectral model parameters here). We are more interested, however, in the variability of the covariance matrices that results from the use of Eq. (6). Figure 7 shows the efficiency of the proposed simplified model in recovering the variability in the covariance matrix of the along-wind turbulence field for the 7×7 square grid in Fig. 3. The figure on the left shows "target" coefficient of variation (COV) estimates, $\bar{c}_{ij}$, at grid point (i, j) of Fig. 3, based on the twenty sample covariance matrices from simulations. These estimates represent the propagation

of uncertainty from spectral model parameter simulations to joint second-moment statistics of the turbulence field. The figure on the right shows corresponding COV estimates, c_{ij}, based on the model described by Eq. (6) which uses a reduced-order three-POD mode representation (i.e., $M = 3$). No variability in the fourth and higher modes (of the forty-nine modes in total) nor in any of the mode shapes is modeled. On comparing the two figures, only slight differences between the target and the approximate COV estimates are seen. This serves to verify the assumption of lack of importance in mode shape variability as well as in the POD energy proportions in the higher modes.

Figure 8 shows the rate of convergence to the target COV estimates based on reconstructed covariance matrices that are based on Eq. (6) using $M = 1, 2, \ldots, 20$. The L_2 norm used to quantify the error in the lower triangular portion of the covariance matrix is defined as $L_2 = \frac{1}{n}\sum_{i=1}^{N}\sum_{j=1}^{i}\sqrt{\left(\frac{c_{ij}-\bar{c}_{ij}}{\bar{c}_{ij}}\right)^2}$ where N is the number of grid points (49, here), while n is the total number of elements in the lower triangular portion of the covariance matrix (which is equal to $49 \times (49+1)/2 = 1,225$ here). Note, from Fig. 8, that the L_2 error norm is less than 2% with as few as three modes. (The error norm stays at this level even when a large number of modes are included because of the "mean" mode shape assumption.) Even with a single mode (i.e., $M = 1$), the L_2 error norm is less than 5%. These results are encouraging and suggest that the variability in second-moment statistics as evidenced by estimates of variability in the covariance matrix for the along-wind turbulence field can be approximated fairly accurately by correctly including the variability in the energy contributions of the first few POD modes only. They also confirm that by disregarding variability in all mode shapes and in the energy from higher modes, no large errors are introduced. This is especially important since eigenmode variability, if it were significant, would have been more cumbersome to model since this variability is associated with a vector (a mode shape), not a scalar random variable which is easier to represent in any simplified scheme. In summary, then, it is sufficient to only estimate the "mean" mode shapes, $\bar{\phi}_j$, the distribution of the total kinetic energy, E, and the proportion of energy in the first few normalized eigenvalues, α_j, in order to accurately represent along-wind inflow turbulence field with inherent variability arising from uncertainties in inflow spectral model parameters.

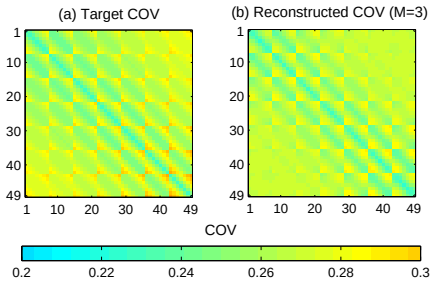

Figure 7. COV estimates for elements, $\bar{c}_{ij}$, of the target covariance matrix (left) and for elements, c_{ij}, of the reconstructed covariance matrix based on three POD modes (right) for the along-wind turbulence component at each grid point (i, j) of Fig. 3.

An implication of the findings in this section is that the uncertainty in parameters of the model by Solari and Piccardo[4] might, in general, influence only portions of a reduced-order POD representation—namely, the lower mode energy contributions. We also saw earlier that turbine load variability is in general reduced relative to the variability in the spectral model parameters. The connection between the reduced load variability and the adequacy of simplified reduced-order POD representations needs to be studied further by examining variability in loads derived using a model such as is suggested by Eq. (6) for simulating inflow turbulence. Such a simplified model might possibly be useful in efficient simulation of appropriate inflow turbulence (with considerations for variability in spectral model parameters, when appropriate) that can then be used to estimate turbine loads.

IV. Conclusions

Variability in turbulence characteristics on a vertical plane with spatial dimensions corresponding to that of the 70-meter diameter rotor of the 1.5MW WindPACT[5] turbine model was investigated. When uncertainty in parameters of the unified turbulence model of Solari and Piccardo[4] was included, significant variability in cross-power spectral density matrices and corresponding covariance matrices was found to result. Also investigated was the influence of these flow uncertainties on statistics of turbine loads including the out-of-plane bending moment at the blade root, the fore-aft tower bending moment at the base, and the yaw bending moment at the tower top of the WindPACT turbine. It was found that variability in turbine load statistics was generally smaller than the variability in the inflow parameters. Of the various loads studied, yaw loads exhibited greater variability which was due to the dependence of these loads on inflow

parameters with especially high variability (i.e., a 40% coefficient of variation).

In a separate but related study, Proper Orthogonal Decomposition (POD) techniques were adopted to help characterize the variability in the covariance matrix of the turbulence random field. The POD analyses indicated very small variations in the mode shapes of the most dominant eigenmodes when simulation studies were carried out. On the other hand, POD eigenvalues, related to the kinetic energy contributions from the different eigenmodes, exhibited relatively greater variability especially for the first few modes. By taking advantage of efficiencies inherent in the POD procedure, a simplified approach was developed for modeling the uncertainties in the inflow turbulence field. Variability in mode shapes as well as in the (normalized) kinetic energy of higher, less energetic POD modes was ignored by employing only "mean" estimates in each case. Full variability in the total kinetic energy and in the energy proportions (normalized eigenvalues) of the first few dominant POD modes was modeled. The efficiency and simplicity of the proposed model in accurately accounting for variability in the along-wind turbulence field that arises from uncertainty in spectral model parameters was illustrated using simulations over the WindPACT turbine rotor plane again. Results showed that by including variability in the total kinetic energy and in the proportion of energy carried by the first three modes (out of a total of forty-nine), while completely ignoring the variability in all mode shapes, an error norm defined in terms of coefficient of variation estimates for the reconstructed and the target covariance matrix could be reduced to approximately 2%. Reduced-order POD representations were shown to be useful in retaining the variability in inflow turbulence fields that arises from uncertainty in parameters used to define power spectra and coherence functions. It is hoped that, with additional studies, an inflow turbulence simulation procedure based on POD techniques might be possible since such a procedure would be able to reasonably accurately represent the influence of such model parameter uncertainty.

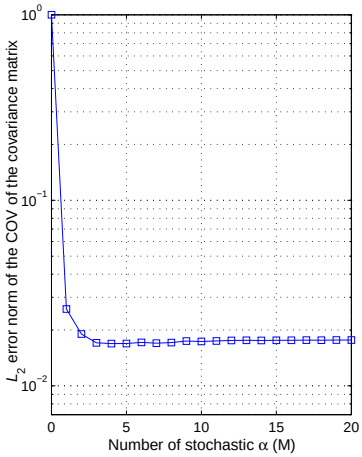

Figure 8. Estimates of the L_2 error norm of the COV of the reconstructed sample covariance matrix of the along-wind turbulence component for different numbers of POD modes.

V. Appendix

Mathematical expressions of the cross-power spectral density functions that describe second-order statistics of the three-dimensional atmospheric turbulence field based on the unified turbulence model[4] employed in the numerical examples are summarized here. More complete derivations and detailed summaries on the statistics for all the inflow turbulence model parameters may be found in the study of Solari and Piccardo.[4]

A. Power spectral density function

The power spectral density function, $S_{\epsilon\epsilon}$, for any turbulence component, ϵ, is modeled as:

$$\frac{fS_{\epsilon\epsilon}(z;f)}{\sigma_\epsilon^2} = \frac{d_\epsilon f L_\epsilon(z)/\bar{u}(z)}{[1+1.5d_\epsilon f L_\epsilon(z)/\bar{u}(z)]^{5/3}}; \quad \epsilon = u, v, \text{or } w$$

where f is the frequency; z is the elevation above the ground. Also, d_ϵ is treated as a constant for each turbulence component, i.e., $d_u = 6.868$, $d_v = d_w = 9.434$. The mean wind velocity, $\bar{u}(z)$, at elevation, z, is assumed to follow a logarithmic profile; thus, $\bar{u}(z) = 2.5u_\star \ln(z/z_0)$ where $u_\star$ and z_0 are fixed (deterministic) values of the friction velocity and the roughness length, respectively. The variance, σ_ϵ^2, of each turbulence component, ϵ, is expressed in terms of a random variable, β_ϵ, and the friction velocity, i.e., $\sigma_\epsilon^2 = \beta_\epsilon u_\star^2$. Similarly, $L_\epsilon(z)$, the integral length scale at elevation z for each turbulence component, ϵ, is expressed as a function of a random variable, ξ_ϵ, and the friction velocity, i.e., $L_\epsilon(z) = 300\xi_\epsilon(z/200)^{(0.67+0.05\ln(z_0))}$, where z, z_0, and $L_\epsilon(z)$ are all expressed in meters.

B. Space coherence function

The space coherence function, $\Omega_{\epsilon\epsilon}$, describes the frequency-dependent cross-correlation of a single turbulence components, ϵ, at different arbitrary points in three-dimensional space. If these two points, A and A', are

located at elevations, z and z', respectively, and have Cartesian coordinates, $\boldsymbol{r}$ and $\boldsymbol{r}'$, respectively, relative to a fixed reference point, the space coherence function for turbulence component, ϵ, may be expressed as:

$$\Omega_{\epsilon\epsilon}(A, A'; f) = \exp\{-\frac{2fC_{r\epsilon}|\boldsymbol{r} - \boldsymbol{r}'|}{\bar{u}(z) + \bar{u}(z')}\}; \quad \epsilon = u, v, \text{or } w; \quad r = x, y, \text{or } z$$

where $C_{r\epsilon}$ is an exponential decay coefficient for the turbulence component, ϵ, in the direction, r. Note that $C_{r\epsilon}$ is treated as a random variable.

C. Point coherence function

The point coherence function, $\Gamma_{\epsilon\eta}$, describes the frequency-dependent cross-correlation between two different turbulence components, ϵ and η ($\epsilon \neq \eta$), at the same point in space and at a specified elevation, z.

$$\Gamma_{uw}(z; f) = -\frac{1}{\kappa_{uw}} \frac{1}{\sqrt{1 + 0.4[fL_u(z)/\bar{u}(z)]^2}};$$

$$\Gamma_{uv}(z; f) = \Gamma_{vw}(z; f) = 0$$

where, as an approximation, it is reasonable to assume that $\kappa_{uw}(z) = 1.11\sqrt{\beta_u(z)\beta_w(z)}[L_w(z)/L_u(z)]^{0.21}$. Also, β_ϵ, κ_{uw}, and L_ϵ are treated as random variables.

D. Cross-power spectral density function

Solari and Piccardo[4] assumed that the coherence function, $\text{coh}_{\epsilon\eta}$, between two dissimilar turbulence components, ϵ and η, at two distinct locations, A and A', can be expressed as:

$$\text{coh}_{\epsilon\eta}(A, A'; f) = \text{sgn}(\Gamma_{\epsilon\eta})\sqrt{\Gamma_{\epsilon\eta}(z; f)\Gamma_{\epsilon\eta}(z'; f)}\sqrt{\Omega_{\epsilon\epsilon}(A, A'; f)\Omega_{\eta\eta}(A, A'; f)}; \quad \epsilon, \eta = u, v, \text{or } w; \quad \epsilon \neq \eta$$

The cross-power spectral density function, $S_{\epsilon\eta}$, can now be generally written using the following relationship:

$$S_{\epsilon\eta}(A, A'; f) = \sqrt{S_{\epsilon\epsilon}(z; f)S_{\eta\eta}(z'; f)}\text{coh}_{\epsilon\eta}(A, A'; f).$$

E. Statistics of model parameters

Employing experimental data, Solari and Piccardo[4] provided expressions for the mathematical expectation, $E[\,]$, the variance, $Var[\,]$, and, where appropriate, the covariance matrix, $\mathbf{C}[\,]$, of various model parameters as follows.

1. Turbulence intensity factors, β_ϵ

Let $\boldsymbol{\beta}$ be $\{\beta_u, \beta_v, \beta_w\}^T$.

$$E[\boldsymbol{\beta}] = \Big(6 - 1.1\arctan[\ln(z_0) + 1.75]\Big)\begin{Bmatrix} 1.00 \\ 0.55 \\ 0.25 \end{Bmatrix}; \quad \mathbf{C}[\boldsymbol{\beta}] = E^2[\beta_u]\begin{bmatrix} 0.0625 & 0.0350 & 0.0155 \\ 0.0350 & 0.0325 & 0.0105 \\ 0.0155 & 0.0105 & 0.0065 \end{bmatrix}$$

2. Integral length scale parameters, ξ_ϵ

Let $\boldsymbol{\xi}$ be $\{\xi_u, \xi_v, \xi_w\}^T$.

$$E[\boldsymbol{\xi}] = \begin{Bmatrix} 1.00 \\ 0.25 \\ 0.10 \end{Bmatrix}; \quad \mathbf{C}[\boldsymbol{\xi}] = \begin{bmatrix} 0.0625 & 0.0155 & 0.0060 \\ 0.0155 & 0.0095 & 0.0025 \\ 0.0060 & 0.0025 & 0.0015 \end{bmatrix}$$

3. Point cross-coherence scaling factor, κ_{uw}

$$E[\kappa_{uw}] \simeq 0.35E[\beta_u]; \quad Var[\kappa_{uw}] \simeq 0.01E^2[\beta_u]$$

4. Exponential decay coefficients, $C_{r\epsilon}$

	C_{xu}	C_{xv}	C_{xw}	C_{yu}	C_{yv}	C_{yw}	C_{zu}	C_{zv}	C_{zw}
Mean, $E[\,]$	3.0	3.0	0.5	10.0	6.5	6.5	10.0	6.5	3.0
COV	0.4	0.6	0.4	0.4	0.6	0.4	0.2	0.2	0.2

Note that COV refers to the coefficient of variation. The covariance between $C_{r\epsilon}$ and $C_{s\eta}$ may be expressed as $C[C_{r\epsilon}, C_{s\eta}] = \rho[C_{r\epsilon}, C_{s\eta}] \cdot \sqrt{Var[C_{r\epsilon}] \cdot Var[C_{s\eta}]}$ where $Var[C_{r\epsilon}] = [\mathrm{COV}[C_{r\epsilon}] \cdot E[C_{r\epsilon}]]^2$ and the correlation coefficient, $\rho[C_{r\epsilon}, C_{s\eta}]$, is assumed to be 0.5 in the model.

In summary, the cross-power spectral density function based on the model by Solari and Piccardo[4] is a function of two (assumed) deterministic inputs—the friction velocity, $u_\star$, and the roughness length, z_0. Additionally, β_ϵ, ξ_ϵ, κ_{uw}, and $C_{r\epsilon}$ are all treated as random variables and generally require at least the roughness length, z_0, in order to obtain their first two statistical moments.

Acknowledgments

The authors gratefully acknowledge the financial support provided by Grant No. 30914 from Sandia National Laboratories and by a CAREER Award (No. CMS-0449128) from the National Science Foundation.

References

[1]IEC, "Wind Turbine Generator System Part 1: Safety Requirements," IEC/TC–88–61400–1, 1998.

[2]Kelley, N., Shirazi, M., Jager, D., Wilde, S., Adams, J., Buhl, M., Sullivan, P., and Patton, E., "Lamar Low-Level Jet Program — Interim Report," NREL/TP–500–34593, National Renewable Energy Laboratory, Golden, CO, 2004.

[3]Kelley, N., Bonnie, J., Scott, G. N., Bialasiewicz, J. T., and Redmond, L. S., "The Impact of Coherent Turbulence on Wind Turbine Aeroelastic Response and its Simulation," NREL/CP–500–38074, National Renewable Energy Laboratory, Golden, CO, 2005.

[4]Solari, G. and Piccardo, G., "Probabilistic 3-D Turbulence Modeling for Gust Buffeting of Structures," *Probabilistic Engineering Mechanics*, Vol. 16, No. 1, 2001, pp. 73–86.

[5]Malcolm, D. J. and Hansen, A. C., "WindPACT Turbine Rotor Design Study," NREL/SR–500–32495, Aug. 2002.

[6]Saranyasoontorn, K. and Manuel, L., "Low-Dimensional Representations of Inflow Turbulence and Wind Turbine Response using Proper Orthogonal Decomposition," *Journal of Solar Energy Engineering*, Vol. 127, No. 4, 2005.

[7]Spitler, J. E., Morton, S. A., Naughton, J. W., and Lindberg, W. R., "Initial Studies of Low-Order Turbulence Modeling of the Wind Turbine In-flow Environment," *Proceedings of the ASME Wind Energy Symposium*, AIAA, Reno, NV, 2004, pp. 442–451.

[8]Lindberg, W. R., Spitler, J. E., and Naughton, J. W., "Modal Structure of Surface Turbulence usign Low-order Turbulence Modeling," *Proceedings of the ASME Wind Energy Symposium*, AIAA, Reno, NV, 2005, pp. 499–509.

[9]Davenport, A. G., "The Spectrum of Hori-zontal Gustiness near the Ground in High Winds," *Quart. J. Roy. Met. Soc.*, Vol. 87, 1961, pp. 194–211.

[10]McKay, M. D., Conover, W. J., and Beckman, R. J., "A Comparison of Three Methods for Selecting Values of Input Variables in the Analysis of Output from a Computer Code," *Technometrics*, Vol. 21, 1979, pp. 239–245.

[11]Veers, P. S., "Three-dimensional Wind Simulation," SANDIA–80–0512, Sandia National Laboratory, Albuquerque, New Mexico, 1988.

[12]Jonkman, J. M. and Buhl Jr., M. L., "FAST User's Guide," NREL/EL–500–38230, National Renewable Energy Laboratory, Golden, CO, 2005.

[13]Hansen, A. C., "Yaw Dynamics of Horizontal Axis Wind Turbines," NREL/TP–442–4822, National Renewable Energy Laboratory, Golden, CO, 1992.

[14]Lumley, J. L., *Stochastic Tools in Turbulence*, Academic Press, New York, 1970.

[15]Holmes, P., Lumley, J. L., and Berkooz, G., *Turbulence, Coherent Structures, Dynamical Systems and Symmetry*, Cambridge Monogr. Mech., Cambridge University Press, 1996.

[16]Jolliffe, I. T., *Principal Component Analysis*, Springer-Verlag, New York, 2nd ed., 2002.